Research Article

Nano Research
2022, 15(6): 5746–5751

ISSN 1998-0124 CN 11-5974/O4
https://doi.org/10.1007/s12274-022-4141-9

Lattice strain suppresses point defect formation in halide perovskites

Caner Deger[1,2], Shaun Tan[3], K. N. Houk[1] (✉), Yang Yang[3] (✉), and Ilhan Yavuz[2] (✉)

[1] *Department of Chemistry and Biochemistry, University of California, Los Angeles, California 90095, USA*
[2] *Department of Physics, Marmara University, Ziverbey, Istanbul 34722, Turkey*
[3] *Department of Materials Science and Engineering and California NanoSystems Institute, University of California Los Angeles, Los Angeles, California 90095, USA*

© Tsinghua University Press 2022

Received: 30 September 2021 / **Revised:** 4 January 2022 / **Accepted:** 4 January 2022

ABSTRACT

We computationally investigate the impact of crystal strain on the formation of native point defects likely to be formed in halide perovskites; A-site cation antisite (I_A), Pb antisite (I_{Pb}), A-site cation vacany (V_A), I vacancy (V_I), Pb vacancy (V_{Pb}), and I interstitial (I_i). We systematically identify compressive and tensile strain to $CsPbI_3$, $FAPbI_3$, and $MAPbI_3$ perovskite structures. We observe that while each type of defect has a unique behaviour, overall, the defect formation in $FAPbI_3$ is much more sensitive to the strain. The compressive strain can enhance the formation energy of neutral I_{Pb} and I_i up to 15% for $FAPbI_3$, depending on the growth conditions. We show that the strain not only controls the formation of defects but also their transition levels in the band gap: A deep level can be transformed into a shallow level by the strain. We anticipate that tailoring the lattice strain can be used as a defect passivation mechanism for future studies.

KEYWORDS

perovskite solar cells, halide perovskites, defect formation, lattice strain

1 Introduction

Since the first generation solid-state perovskite solar cell (PSC) was launched in 2012 [1, 2], hybrid organic–inorganic halide perovskites have received great interests as a low-cost and highly efficient candidate for third generation solar cells (SCs) [3–5]. The power conversion efficiency (PCE) of perovskite solar cells has keenly raised to 25.5% in the lab [6]. The highest PCEs are mostly achieved by employing the organic–inorganic hybrid metal triiodide perovskite (MTP) materials (e.g., formamidinium lead iodide ($FAPbI_3$)) due to their high charge mobility, long charge diffusion length, high absorption coefficient, and tunable band gap [7, 8]. Furthermore, their facile and cost-effective fabrication process can pave the way for large-scale commercialization (>1 cm^2) with high PCE of 20% [9–11] in a decade.

While MTP-based solar cells are competitive with conventional photovoltaics, the large number of defects often present significantly damage the optoelectronic performance of MTP-based solar cells and long-term stability [12, 13]. Intrinsic point defects in semiconductors can be classified into three types: (I) vacancy defects where an atom is missing from one of the lattice sites; (II) Interstitial defects where an atom of the same or of a different type occupies a normally unoccupied site in the lattice. (III) Antisite defects in an ordered alloy or compound when atoms of different type exchange positions. Another classification of the defects is based on the position of their electronic transition levels within the band gap. This position relative to the conduction band minimum (CBM) or valence band maximum (VBM) determines the type of defect trap states as "shallow" or "deep" [14]. Since the crystal growth procedures are always fast and require high temperature, the formation of defects is not rare in MTP, and the defects generally influence the performance of solar cells. Advent of the thermodynamic PCE limit of MTP requires not only a better understanding of the defects, but also research to achieve passivation.

Since the defects have a strong impact on the opto-electronic properties and stability of MTPs, defect passivation has been widely studied [5, 15, 16]. Modifications of the perovskite precursor solution aids both in the growth of highly crystalline perovskite films and in passivation of the grain boundaries of the crystals [17–20]. Similarly, bottom–up defect passivation can introduce nucleation sites to the crsytal, which enhances the crystallization [21, 22] and suppresses the formation of the defects. In contrast to passivating the defect during the growth process, post-treatment of the top surface without affecting their morphologies or causing recrystallization can provide compact and flat perovskite films [20, 23–26].

Along with these strategies, in the past few years, lattice strain is directly associated to both defect concentration [27] and carrier dynamics [28] in MTPs. Perovskites are generally vulnerable to the lattice strain due to their mechanically-soft nature [29]. A stress applied to the crystal leads to a deformation of the lattice resulting a change in lattice parameters. [30] Quantitatively, the ratio of the change in the lattice parameter originated by a stress to the strain-free lattice parameter is defined as "strain". The strain in the lattice can be controlled by both internal and external stress.

Address correspondence to K. N. Houk, houk@chem.ucla.edu; Yang Yang, yangy@ucla.edu; Ilhan Yavuz, ilhan.yavuz@marmara.edu.tr

The internal engineering of the strain in MTPs can be performed by varying the effective radius of A-cations [31, 32] and X-anions [33], quantum dot inclusion [34], and surface reconstruction [35] while the external strain engineering can be achieved by lattice mismatches [36, 37], temperature gradients [28], annealing [38], and bending after film formation [39–41]. While the amount of applied strain by these methods is varied, the typical strain range is ±2%. Macroscopic parameters such as power conversion efficiency and stability are strongly influenced by this amount of strain [33, 37, 42]. Given that MTPs can have 12 native point defects (three vacancies, three interstitials, and six antisite occupations), each defect may behave distinctively against the crystal strain, depending on the A-site cation in $APbI_3$ type MTPs.

We have investigated the influence of lattice strain on the formation energy of commonly-studied 6 native point defects: A-site cation antisite (I_A), Pb antisite (I_{Pb}), A-site cation vacany (V_A), I vacancy (V_I), Pb vacancy (V_{Pb}), and I interstitial (I_i) in $APbI_3$ perovskites; $CsPbI_3$, $FAPbI_3$, and $MAPbI_3$. In addition, we investigated the influence of lattice strain and electrochemical potential on the formation of the selected point defects. The impact of the strain on the transition levels of the defects is also revealed. Our study suggests that lattice strain can be used as an alternative defect passivation method in metal-halide perovskites.

2 Methods

Defect formation energy calculations were performed based on the density functional theory (DFT)-implemented Vienna *ab initio* simulation package (VASP) [43–45]. Generalized gradient approximation (GGA) of Perdew–Burke–Ernzerhof (PBE) type functional for electron–electron interactions and projector augmented wave (PAW) method for electron–ion interactions [46] were employed for the calculations with the cut-off energies for the plane-wave basis sets of 400 eV. PBE is a cost-effective functional when compared to hybrid functionals (such as Heyd–Scuseria–Ernzerhof, (HSE)) giving reasonably consistent results in defect formation energies determined through total energy differences [47, 48]. A supercell with a 3 × 3 × 3 periodicity was used in all cases. A structural relaxation for both ionic positions and cell dimensions was performed to obtain most stable geometry until the residual forces became smaller than 0.05 eV/˚A. Following the geometry optimization, the lattice strain was implemented by changing the lattice parameter along out-of-plane direction: The contraction and expansion of the lattice will be called as compressive and tensile strain, respectively. This uniaxial strain approach allows us to figure out the effect of the ratio between out-of-plane and in-plane lattice constants (c/a) on the defect formation. Most studies on crystal strain focus on this c/a ratio since the lattice-originated phenomena are generally proportional to the c/a ratio [49, 50]. The computations of the defect formation energies are detailed in the Electronic Supplementary Material (ESM).

3 Results and discussion

We varied the crystal strain from −2% (compressive) to 2% (tensile) for $CsPbI_3$, $FAPbI_3$, and $MAPbI_3$ with point defects of I_{A-site}, I_{Pb}, V_{A-site}, V_I, V_{Pb}, and I_i. This 2% strain, for instance, amounts to as much as roughly 0.1 Å variation in a Pb–I bond along the out-of-plane direction. The relative formation energies of neutral defects in strained perovskites with respect to freestanding defective perovskites are given in Figs. 1(a)–1(c). While the given neutral defect formation energies (DFEs) are calculated in moderate growth conditions, DFEs for Pb-rich and I-rich conditions are also presented in Figs. 1(d)–1(f) for comparison. Also, the formation energies of investigated defects for I-rich and Pb-rich conditions can be found in the ESM. In Fig. 1(a), we show that a compressive strain in $CsPbI_3$ can further stabilize the DFE of V_{Cs} up to 7%. Considering that the DFE of V_{Cs} is relatively small (Fig. 1(d)), i.e., the defect formation is quite possible under certain conditions, and the control of the lattice strain becomes crucial. On the other hand, the DFE of V_I is increased as much as 4%, which can reduce the formation of V_I. The unique behavior of V_I in Fig. 1(a) can be associated with its charge-state as it is the sole electron–donor defect we studied. Indeed, the center of defected unit cell undergoes a significant contraction along the *x*-direction due to electron donation, resulting an enhancement in defect formation energy by the compressive strain. Furthermore, V_{Cs}, I_{Cs}, V_{Pb}, and I_i cause an expansion along the *x*-direction and their DFEs are reduced for compressive strain. Lastly, I_{Pb} has no effect on the crystal structure and prognostically the DFE is insensitive to the lattice strain. Thus, we can admit that the distortion in which the defect is located can be restored by the lattice strain. Among the A-site cations and defects under study, FA-type forms the most strain-sensitive halide perovskite (see Fig. 1(b)) in which the DFEs can increase up to ~ 20% relatively by the lattice strain. Even if $MAPbI_3$ is also sensitive to the strain for V_{Pb} and V_{MA} (see Fig. 1(c)), the maximum relative DFE is around 8%, which is still far below the relative DFEs calculated for $FAPbI_3$. In general, defects were stabilized (destabilized) by increasing compressive (tensile)

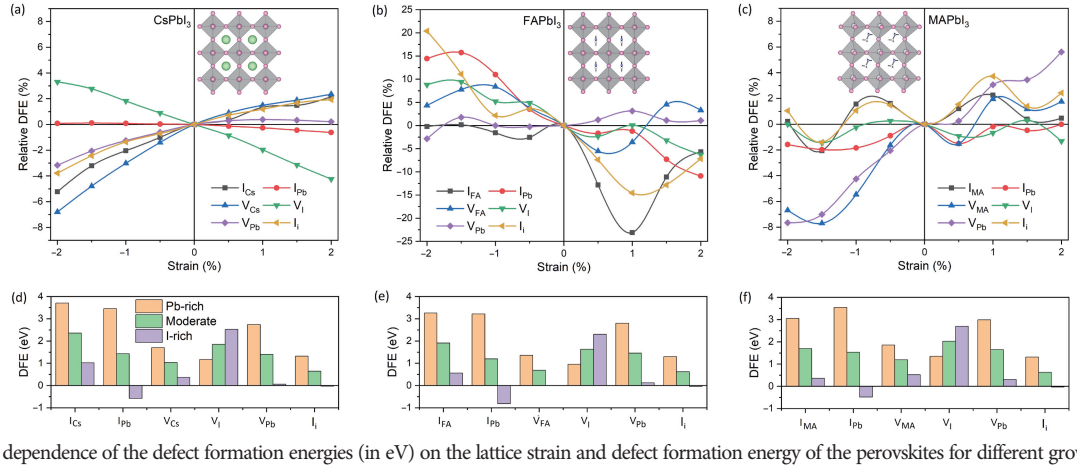

Figure 1 The dependence of the defect formation energies (in eV) on the lattice strain and defect formation energy of the perovskites for different growth conditions. The relative DFE with respect to the strain for selected neutral intrinsic defects (I_A, I_{Pb}, V_A, V_I, V_{Pb}, and I_i) in (a) $CsPbI_3$, (b) $FAPbI_3$, and (c) $MAPbI_3$ perovskites under moderate conditions. The negative value of % indicates compressive strain while positive % values correspond to tensile strain along the out-of-plane direction throughout the study. The formation energies of intrinsic point defects under Pb-rich, moderate, and I-rich conditions in (d) $CsPbI_3$, (e) $FAPbI_3$, and (f) $MAPbI_3$ perovskites.

strain in $CsPbI_3$ and $MAPbI_3$. However, the trend is reversed in $FAPbI_3$ as shown in Figs. 1(a)–1(c). We attribute this behaviour to the large size of the FA molecule relative to Cs and MA, which makes the lattice structure vulnerable to the contractive point defects. In a deterministic manner, the Goldschmidt tolerance factor (t) of $FAPbI_3$ (t_{FAPbI_3} = 0.99) [51] is higher than that of $MAPbI_3$ (t_{MAPbI_3} = 0.91) [51] and $CsPbI_3$ (t_{CsPbI_3} = 0.89) [52]. Since the tolerance factor of $FAPbI_3$ is on the upper border of the cubic perovskite formation zone, $0.8 < t < 1$ [53–55], the defect formation in $FAPbI_3$ is more sensitive to the crystal distortions. The schematic representation of the effect of the strain of the tolerance factor is given in Fig. 2. The tolerance factor of $CsPbI_3$ and $MAPbI_3$ is around the middle of the stable cubic perovskite formation zone. However, $FAPbI_3$ is very close to the hexagonal phase transition area. Applying a compressive strain drifts the tolerance factor down to the stable cubic region, which enhances the formation energy of defects. Moreover, a tensile strain applied to the crystal shifts the tolerance factor to the less-stable phase transition area, which makes it vulnerable to the defect formations.

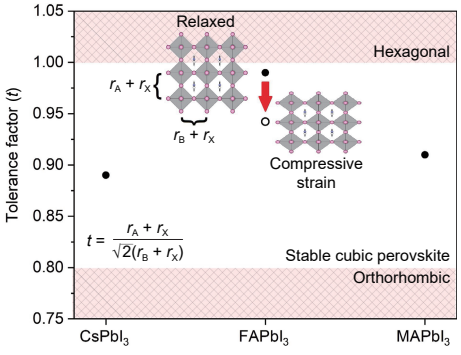

Figure 2 Schematic representation of strain-induced tolerance factor adjustment of $FAPbI_3$. Herein, r_A, r_B, and r_X represent the radii of A-site molecule, B-site metal, and X-site halide in ABX_3 perovskites, respectively. In addition, $r_A + r_X$ shown here is a space-diagonal length. The change in the tolerance factor of $FAPbI_3$ is enlarged to show the influence of the strain.

In addition to the effect of lattice strain, the electrochemical potential has an impact on the formation energy of defects [56]. A concurrent investigation of the influences of lattice strain and electrochemical potential on the formation of the selected point defects is summarized in Fig. 3. The upper heat-maps (Figs. 3(a)–3(c)) present the formation energy of I_{Pb} while middle ones (Figs. 3(d)–3(f)) show those of V_I and lower ones (Figs. 3(g)–3(i)) show those of I_i in $CsPbI_3$, $FAPbI_3$, and $MAPbI_3$, respectively. For I_{Pb}, the formation energy is lower for higher Fermi energies, i.e., I_{Pb} is more stable in an electron-rich environment. On the other hand, V_I is dominant when the host material is p-type ($E_F \sim 0.5$) in Figs. 3(d)–3(f). However, lattice strain plays a crucial role on the heat-maps. For $FAPbI_3$, I_{Pb} is more stable under tensile strain in Fig. 3(b). Similarly, the tensile strain linearly shifts the stable region of V_I towards higher fermi energies in Fig. 3(d). As a result, the lattice strain more or less influences the formation probability of the selected defects in the host material. Aside from the defect formation energies, the photovoltaic performance of perovskites is also associated with the charge-state transition levels. The Fermi level where the defect state can accept/donate electrons is called as the transition level of a defect, which can be "shallow" or "deep" according to its position in the band gap. The calculated transition

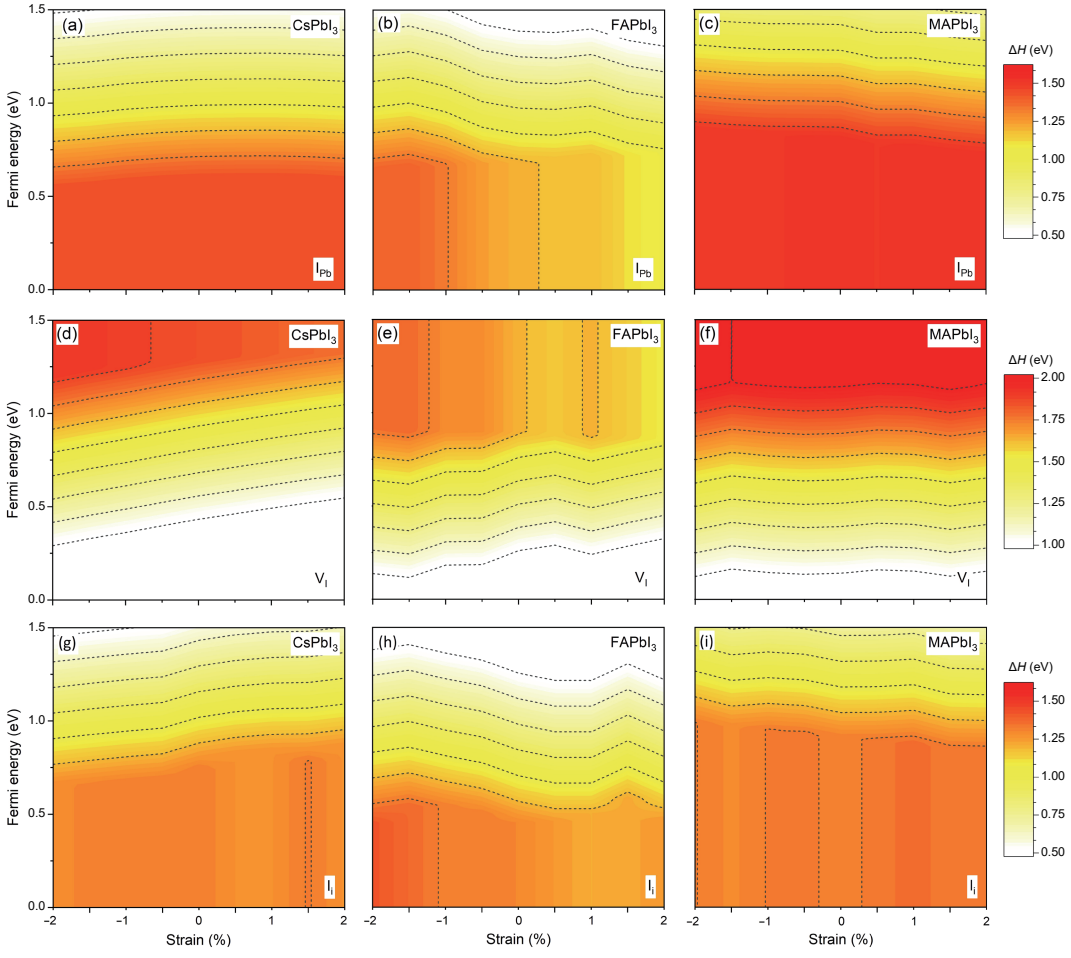

Figure 3 The dependence of the defect formation energies on the Fermi energy and lattice strain, concurrently. The formation energy of I_{Pb} is given in (a) $CsPbI_3$, (b) $FAPbI_3$, and (c) $MAPbI_3$ while that of V_I is shown in (d) $CsPbI_3$, (e) $FAPbI_3$, and (f) $MAPbI_3$ and that of I_i is shown in (g) $CsPbI_3$, (h) $FAPbI_3$, and (i) $MAPbI_3$ perovskites.

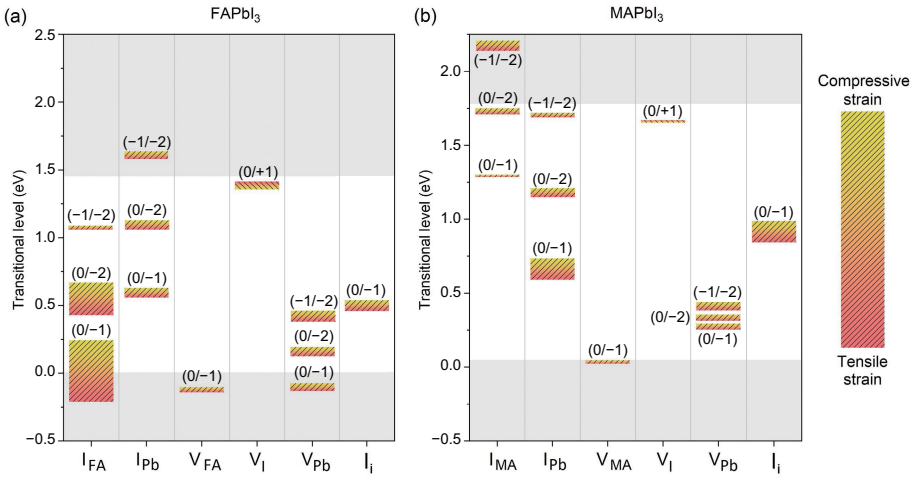

Figure 4 The charge transition energy levels of selected intrinsic defects in (a) $FAPbI_3$, and (b) $MAPbI_3$. The influence of lattice strain on the transition levels is shown by the color gradient. The strain is varied from −2% (compressive) to 2% (tensile)

levels for the point defects of I_{A-site}, I_{Pb}, V_{A-site}, V_I, V_{Pb}, and I_i in $FAPbI_3$, and $MAPbI_3$ are respectively shown in Figs. 4(a) and 4(b). The transition levels of all investigated defects are affected by the lattice stain in a certain degree. The strain controls the transition level of a defect in the band gap and even a deep defect can be transformed into a shallow defect by the strain: A tensile strain applied to the $FAPbI_3$ transforms the deep defect of I_{FA} into a shallow one in Fig. 4(a). The crystal strain influences not only the formation energy of defects but also the electronic band structure of the crystal and finally the transitional level of the defects. Moreover, some alterations in the bandgap have been recently reported by Ghosh et al. [57] and Qiao et al. [58]. Considering that some halide perovskites naturally become strained as-grown or after annealing, the defects that are considered harmful in the freestanding lattice case may actually be benign under strain, vice versa. Also, tailoring the lattice strain by proper substrates and/or buffer layers can play a role in the formation and alteration of transition level of defects as well as other defect passivation methods.

4 Summary

In summary, the impact of lattice strain on the defect properties of $CsPbI_3$, $FAPbI_3$, and $MAPbI_3$ perovskite solar cells has been systematically studied via first-principles calculations. It is found that defect formation in $FAPbI_3$ is very sensitive to the strain, and the defect formation energy can be enhanced up to ~ 20% by a compressive strain. We attribute this behavior to the tolerance factor drifted down to the stable cubic perovskite region. According to the concurrent investigation of the influences of lattice strain and electrochemical potential on the defect formation, we found that the lattice strain more or less influences the formation probability of defects in the host material. Moreover, the strain manipulates the transition level of the defects in the band gap and even can transform a deep defect into a shallow defect. We suggest the usage of lattice strain as a defect passivation method.

Acknowledgments

The numerical calculations reported in this paper were performed at TUBITAK ULAKBIM, High Performance and Grid Computing Center (TRUBA resources) and Hoffman2 cluster at the University of California, Los Angeles. Computational analysis was performed at the Simulations and Modelling Research Lab (Simulab), Physics Department of MU. C. D. would like to thank the Fulbright Turkey Commission for providing a valuable scholarship for his post-doctoral study at the United States. K. N. H. was supported by the National Science Foundation (CHE-1764328). S. T. and Y. Y. were supported by the U.S. Department of Energy's Office of Energy Efficiency and Renewable Energy (EERE) under the Solar Energy Technologies Office under award DE-EE0008751.

Electronic Supplementary Material: Supplementary material (formation energies of I_A, I_{Pb}, V_A, V_I, V_{Pb}, and I_i in $APbI_3$ perovskites; $CsPbI_3$, $FAPbI_3$, and $MAPbI_3$ with respect to the strain for moderate, I-rich, and Pb-rich growth conditions, computational details related to the calculation of defect formation energy, chemical potential calculations, and energy corrections) is available in the online version of this article at https://doi.org/10.1007/s12274-022-4141-9.

References

[1] Kim, H. S.; Lee, C. R.; Im, J. H.; Lee, K. B.; Moehl, T.; Marchioro, A.; Moon, S. J.; Humphry-Baker, B.; Yum, J. H.; Moser, J. E. et al. Lead iodide perovskite sensitized all-solid-state submicron thin film mesoscopic solar cell with efficiency exceeding 9%. *Sci. Rep.* **2012**, *2*, 591.

[2] Lee, M. M.; Teuscher, J.; Miyasaka, T.; Murakami, T. N.; Snaith, H. J. Efficient hybrid solar cells based on meso-superstructured organometal halide perovskites. *Science* **2012**, *338*, 643–647.

[3] Snaith, H. J. Present status and future prospects of perovskite photovoltaics. *Nat. Mater.* **2018**, *17*, 372–376.

[4] Saliba, M.; Matsui, T.; Seo, J. Y.; Domanski, K.; Correa-Baena, J. P.; Nazeeruddin, M. K.; Zakeeruddin, S. M.; Tress, W.; Abate, A.; Hagfeldt, A. et al. Cesium-containing triple cation perovskite solar cells: Improved stability, reproducibility and high efficiency. *Energy Environ. Sci.* **2016**, *9*, 1989–1997.

[5] Wang, R.; Xue, J. J.; Wang, K. L.; Wang, Z. K.; Luo, Y. Q.; Fenning, D.; Xu, G. W.; Nuryyeva, S.; Huang, T. Y.; Zhao, Y. P. et al. Constructive molecular configurations for surface-defect passivation of perovskite photovoltaics. *Science* **2019**, *366*, 1509–1513.

[6] *Best Research-Cell Efficiency Chart* [Online]. https://www.nrel.gov/pv/cell-efficiency.html (accessed Apr 4, 2021).

[7] Zhao, Y. X.; Zhu, K. Organic-inorganic hybrid lead halide perovskites for optoelectronic and electronic applications. *Chem. Soc. Rev.* **2016**, *45*, 655–689.

[8] Ran, C. X.; Xu, J. T.; Gao, W. Y.; Huang, C. M.; Dou, S. X. Defects in metal triiodide perovskite materials towards high-performance solar cells: Origin, impact, characterization, and engineering. *Chem. Soc. Rev.* **2018**, *47*, 4581–4610.

[9] Li, X.; Bi, D. Q.; Yi, C. Y.; Décoppet, J. D.; Luo, J. S.; Zakeeruddin,

S. M.; Hagfeldt, A.; Grätzel, M. A vacuum flash-assisted solution process for high-efficiency large-area perovskite solar cells. *Science* **2016**, *353*, 58–62.

[10] He, M.; Li, B.; Cui, X.; Jiang, B. B.; He, Y. J.; Chen, Y. H.; O'Neil, D.; Szymanski, P.; EI-Sayed, M. A.; Huang, J. S. et al. Meniscus-assisted solution printing of large-grained perovskite films for high-efficiency solar cells. *Nat. Commun.* **2017**, *8*, 16045.

[11] Li, Z.; Klein, T. R.; Kim, D. H.; Yang, M. J.; Berry, J. J.; Van Hest, M. F. A. M.; Zhu, K. Scalable fabrication of perovskite solar cells. *Nat. Rev. Mater.* **2018**, *3*, 18017.

[12] Ball, J. M.; Petrozza, A. Defects in perovskite-halides and their effects in solar cells. *Nat. Energy* **2016**, *1*, 16149.

[13] Tan, S. Yavuz, I.; Weber, M. H.; Huang, T. Y.; Chen, C. H.; Wang, R.; Wang, H. C.; Ko, J. H.; Nuryyeva, S.; Xue, J. J. et al. Shallow iodine defects accelerate the degradation of α-phase formamidinium perovskite. *Joule* **2020**, *4*, 2426–2442.

[14] Queisser, H. J.; Haller, E. E. Defects in semiconductors: Some fatal, some vital. *Science* **1998**, *281*, 945–950.

[15] Zheng, X. P.; Chen, B.; Dai, J.; Fang, Y. J.; Bai, Y.; Lin, Y. Z.; Wei, H. T.; Zeng, X. C.; Huang, J. S. Defect passivation in hybrid perovskite solar cells using quaternary ammonium halide anions and cations. *Nat. Energy* **2017**, *2*, 17102.

[16] Akin, S.; Arora, N.; Zakeeruddin, S. M.; Grätzel, M.; Friend, R. H.; Dar, M. I. New strategies for defect passivation in high-efficiency perovskite solar cells. *Adv. Energy Mater.* **2020**, *10*, 1903090.

[17] Song, L.; Guo, X. Y.; Hu, Y. S.; Lv, Y.; Lin, J.; Liu, Z. Q.; Fan, Y.; Liu, X. Y. Efficient inorganic perovskite light-emitting diodes with polyethylene glycol passivated ultrathin $CsPbBr_3$ films. *J. Phys. Chem. Lett.* **2017**, *8*, 4148–4154.

[18] Wang, N. N.; Cheng, L.; Ge, R.; Zhang, S. T.; Miao, Y. F.; Zou, W.; Yi, C.; Sun, Y.; Cao, Y.; Yang, R. et al. Perovskite light-emitting diodes based on solution-processed self-organized multiple quantum wells. *Nat. Photon.* **2016**, *10*, 699–704.

[19] Yuan, M. J.; Quan, L. N.; Comin, R.; Walters, G.; Sabatini, R.; Voznyy, O.; Hoogland, S.; Zhao, Y. B.; Beauregard, E. M.; Kanjanaboos, P. et al. Perovskite energy funnels for efficient light-emitting diodes. *Nat. Nanotechnol.* **2016**, *11*, 872–877.

[20] Lee, S. Kim, D. B.; Yu, J. C.; Jang, C. H.; Park, J. H.; Lee, B. R.; Song, M. H. Versatile defect passivation methods for metal halide perovskite materials and their application to light-emitting devices. *Adv. Mater.* **2019**, *31*, 1805244.

[21] Wang, N. N.; Cheng, L.; Si, J. J.; Liang, X. Y.; Jin, Y. Z.; Wang, J. P.; Huang, W. Morphology control of perovskite light-emitting diodes by using amino acid self-assembled monolayers. *Appl. Phys. Lett.* **2016**, *108*, 141102.

[22] Zou, Y. T.; Ban, M. Y.; Yang, Y. G.; Bai, S.; Wu, C.; Han, Y. J.; Wu, T.; Tan, Y. S.; Huang, Q.; Gao, X. Y. et al. Boosting perovskite light-emitting diode performance via tailoring interfacial contact. *ACS Appl. Mater. Interfaces* **2018**, *10*, 24320–24326.

[23] DeQuilettes, D. W.; Koch, S.; Burke, S.; Paranji, R. K.; Shropshire, A. J.; Ziffer, M. E.; Ginger, D. S. Photoluminescence lifetimes exceeding 8 μs and quantum yields exceeding 30% in hybrid perovskite thin films by ligand passivation. *ACS Energy Lett.* **2016**, *1*, 438–444.

[24] Lee, S.; Park, J. H.; Lee, B. R.; Jung, E. D.; Yu, J. C.; Di Nuzzo, D.; Friend, R. H.; Song, M. H. Amine-based passivating materials for enhanced optical properties and performance of organic-inorganic perovskites in light-emitting diodes. *J. Phys. Chem. Lett.* **2017**, *8*, 1784–1792.

[25] Yang, X. L.; Zhang, X. W.; Deng, J. X.; Chu, Z. M.; Jiang, Q.; Meng, J. H.; Wang, P. Y.; Zhang, L. Q.; Yin, Z. G.; You, J. B. Efficient green light-emitting diodes based on quasi-two-dimensional composition and phase engineered perovskite with surface passivation. *Nat. Commun.* **2018**, *9*, 570.

[26] Jamaludin, N. F.; Yantara, N.; Ng, Y. F.; Li, M. J.; Goh, T. W.; Thirumal, K.; Sum, T. C.; Mathews, N.; Soci, C.; Mhaisalkar, S. Grain size modulation and interfacial engineering of $CH_3NH_3PbBr_3$ emitter films through incorporation of tetraethylammonium bromide. *ChemPhysChem* **2018**, *19*, 1075–1080.

[27] Jones, T. W.; Osherov, A.; Alsari, M.; Sponseller, M.; Duck, B. C.; Jung, Y. K.; Settens, C.; Niroui, F.; Brenes, R.; Stan, C. V. et al. Lattice strain causes non-radiative losses in halide perovskites. *Energy Environ. Sci.* **2019**, *12*, 596–606.

[28] Zhu, C.; Niu, X. X.; Fu, Y. H.; Li, N. X.; Hu, C.; Chen, Y. H.; He, X.; Na, G. R.; Liu, P. F.; Zai, H. C. et al. Strain engineering in perovskite solar cells and its impacts on carrier dynamics. *Nat. Commun.* **2019**, *10*, 815.

[29] Moloney, E. G.; Yeddu, V.; Saidaminov, M. I. Strain engineering in halide perovskites. *ACS Mater. Lett.* **2020**, *2*, 1495–1508.

[30] Wang, J. T. W.; Wang, Z. P.; Zhang, W.; deQuilettes, D. W.; Wisnivesky-Rocca-Rivarola, F.; Huang, J.; Nayak, P. K.; Patel, J. B.; Yusof, H. A. M.; Vaynzof, Y. et al. Efficient perovskite solar cells by metal ion doping. *Energy Environ. Sci.* **2016**, *9*, 2892–2901.

[31] Wu, C.; Chen, K.; Guo, D. Y.; Wang, S. L.; Li, P. G. Cations substitution tuning phase stability in hybrid perovskite single crystals by strain relaxation. *RSC Adv.* **2018**, *8*, 2900–2905.

[32] Tan, S.; Yavuz, I.; De Marco, N.; Huang, T.; Lee, S. J.; Choi, C. S.; Wang, M. H.; Nuryyeva, S.; Wang, R.; Zhao, Y. P. et al. Steric impediment of ion migration contributes to improved operational stability of perovskite solar cells. *Adv. Mater.* **2020**, *32*, 1906995.

[33] Saidaminov, M. I.; Kim, J.; Jain, A.; Quintero-Bermudez, R.; Tan, H. R.; Long, G. K.; Tan, F. R.; Johnston, A.; Zhao, Y. C.; Voznyy, O. et al. Suppression of atomic vacancies via incorporation of isovalent small ions to increase the stability of halide perovskite solar cells in ambient air. *Nat. Energy* **2018**, *3*, 648–654.

[34] Liu, M. X.; Chen, Y. L.; Tan, C. S.; Quintero-Bermudez, R.; Proppe, A. H.; Munir, R.; Tan, H. R.; Voznyy, O.; Scheffel, B.; Walters, G. et al. Lattice anchoring stabilizes solution-processed semiconductors. *Nature* **2019**, *570*, 96–101.

[35] Wang, H.; Zhu, C.; Liu, L.; Ma, S.; Liu, P. F.; Wu, J. F.; Shi, C. B.; Du, Q.; Hao, Y. M.; Xiang, S. S. et al. Interfacial residual stress relaxation in perovskite solar cells with improved stability. *Adv. Mater.* **2019**, *31*, 1904408.

[36] Steele, J. A.; Jin, H. D.; Dovgaliuk, I.; Berger, R. F.; Braeckevelt, T.; Yuan, H. F.; Martin, C.; Solano, E.; Lejaeghere, K.; Rogge, S. M. J. et al. Thermal unequilibrium of strained black $CsPbI_3$ thin films. *Science* **2019**, *365*, 679–684.

[37] Chen, Y. M.; Lei, Y. S.; Li, Y. H.; Yu, Y. G.; Cai, J. Z.; Chiu, M. H.; Rao, R.; Gu, Y.; Wang, C. F.; Choi, W. et al. Strain engineering and epitaxial stabilization of halide perovskites. *Nature* **2020**, *577*, 209–215.

[38] Zhou, Q.; Jin, Z. W.; Li, H.; Wang, J. Z. Enhancing performance and uniformity of $CH_3NH_3PbI_{3-x}Cl_x$ perovskite solar cells by air-heated-oven assisted annealing under various humidities. *Sci. Rep.* **2016**, *6*, 21257.

[39] Rolston, N.; Bush, K. A.; Printz, A. D.; Gold-Parker, A.; Ding, Y. C.; Toney, M. F.; Mcgehee, M. D.; Dauskardt, R. H. Engineering stress in perovskite solar cells to improve stability. *Adv. Energy Mater.* **2018**, *8*, 1802139.

[40] Zhao, J. J.; Deng, Y. H.; Wei, H. T.; Zheng, X. P.; Yu, Z. H.; Shao, Y. C.; Shield, J. E.; Huang, J. S. Strained hybrid perovskite thin films and their impact on the intrinsic stability of perovskite solar cells. *Sci. Adv.* **2017**, *3*, eaao5616.

[41] Wang, C.; Ma, L.; Guo, D. Q.; Zhao, X.; Zhou, Z. L.; Lin, D. B.; Zhang, F. T.; Zhao, W. R.; Zhang, J. H.; Nie, Z. G. Balanced strain-dependent carrier dynamics in flexible organic-inorganic hybrid perovskites. *J. Mater. Chem. C* **2020**, *8*, 3374–3379.

[42] Liu, D. T.; Luo, D. Y.; Iqbal, A. N.; Orr, K. W. P.; Doherty, T. A. S.; Lu, Z. H.; Stranks, S. D.; Zhang, W. Strain analysis and engineering in halide perovskite photovoltaics. *Nat. Mater.* **2021**, *20*, 1337–1346.

[43] Kresse, G.; Hafner, J. *Ab initio* molecular dynamics for liquid metals. *Phys. Rev. B* **1993**, *47*, 558–561.

[44] Kresse, G.; Furthmüller, J. Efficiency of *ab-initio* total energy calculations for metals and semiconductors using a plane-wave basis set. *Comput. Mater. Sci.* **1996**, *6*, 15–50.

[45] Kresse, G.; Furthmuller, J. Efficient iterative schemes for *ab initio* total-energy calculations using a plane-wave basis set. *Phys. Rev. B* **1996**, *54*, 11169.

[46] Kresse, G.; Joubert, D. From ultrasoft pseudopotentials to the projector augmented-wave method. *Phys. Rev. B* **1999**, *59*,

1758–1775.
[47] Komsa, H. P.; Broqvist, P.; Pasquarello, A. Alignment of defect levels and band edges through hybrid functionals: Effect of screening in the exchange term. *Phys. Rev. B* **2010**, *81*, 205118.
[48] Freysoldt, C.; Lange, B.; Neugebauer, J.; Yan, Q. M.; Lyons, J. L.; Janotti, A.; Van De Walle, C. G. Electron and chemical reservoir corrections for point-defect formation energies. *Phys. Rev. B* **2016**, *93*, 165206.
[49] Deger, C. Strain-enhanced dzyaloshinskii-moriya interaction at Co/Pt interfaces. *Sci. Rep.* **2020**, *10*, 12314.
[50] Aksu, P.; Deger, C.; Yavuz, I.; Yildiz, F. Strain-promoted perpendicular magnetic anisotropy in Co-Rh alloys. *Appl. Phys. Lett.* **2020**, *116*, 212402.
[51] Kieslich, G.; Sun, S. J.; Cheetham, A. K. An extended tolerance factor approach for organic-inorganic perovskites. *Chem. Sci.* **2015**, *6*, 3430–3433.
[52] Travis, W.; Glover, E. N. K.; Bronstein, H.; Scanlon, D. O.; Palgrave, R. G. On the application of the tolerance factor to inorganic and hybrid halide perovskites: A revised system. *Chem. Sci.* **2016**, *7*, 4548–4556.
[53] Han, G. F.; Hadi, H. D.; Bruno, A.; Kulkarni, S. A.; Koh, T. M.; Wong, L. H.; Soci, C.; Mathews, N.; Zhang, S.; Mhaisalkar, S. G. Additive selection strategy for high performance perovskite photovoltaics. *J. Phys. Chem. C* **2018**, *122*, 13884–13893.
[54] Fu, Y. P.; Hautzinger, M. P.; Luo, Z. Y.; Wang, F. F.; Pan, D. X.; Aristov, M. M.; Guzei, I. A.; Pan, A. L.; Zhu, X. Y.; Jin, S. Incorporating large a cations into lead iodide perovskite cages: Relaxed goldschmidt tolerance factor and impact on exciton–phonon interaction. *ACS Cent. Sci.* **2019**, *5*, 1377–1386.
[55] Li, Z.; Yang, M. J.; Park, J. S.; Wei, S. H.; Berry, J. J.; Zhu, K. Stabilizing perovskite structures by tuning tolerance factor: Formation of formamidinium and cesium lead iodide solid-state alloys. *Chem. Mater.* **2016**, *28*, 284–292.
[56] Liu, N.; Yam, C. First-principles study of intrinsic defects in formamidinium lead triiodide perovskite solar cell absorbers. *Phys. Chem. Chem. Phys.* **2018**, *20*, 6800–6804.
[57] Ghosh, D.; Aziz, A.; Dawson, J. A.; Walker, A. B.; Islam, M. S. Putting the squeeze on lead iodide perovskites: Pressure-induced effects to tune their structural and optoelectronic behavior. *Chem. Mater.* **2019**, *31*, 4063–4071.
[58] Qiao, L.; Fang, W. H.; Long, R.; Prezhdo, O. V. Elimination of charge recombination centers in metal halide perovskites by strain. *J. Am. Chem. Soc.* **2021**, *143*, 9982–9990.